Frictional and wear properties of cobalt/multiwalled carbon nanotube composite films formed by electrodeposition

Susumu Arai*, Kazuaki Miyagawa

Department of Chemistry and Material Engineering, Faculty of Engineering, Shinshu University, 4-17-1 Wakasato, Nagano 380-8553, Japan

* Corresponding author
Tel: +81-26-269-5413
Fax: +81-26-269-5432
E-mail address: araisun@shinshu-u.ac.jp (S. Arai)

Abstract

Carbon nanotubes (CNTs) have solid lubricity due to their unique structure and as such, CNT composites are also expected to exhibit superior tribological properties. In this study, Co/CNT composite films were fabricated using a composite electrodeposition technique and their tribological properties were investigated. Three different sizes of multiwalled carbon nanotubes (MWCNTs) were used as CNTs. The microstructures of the composite films were examined using scanning electron microscopy. Frictional and wear properties were examined using a ball-on-disk method without any lubricants at room temperature and at high temperatures (100-500 °C). The Co/MWCNT composite films had lower coefficients of friction than a cobalt film at room temperature. In contrast, the coefficients of friction of the Co/MWCNT composite film at high temperature became higher than that at room temperature and slightly lower than that of a cobalt film.

Key Words: Multiwalled carbon nanotube; Cobalt; composite; Electrodeposition; Frictional properties; High temperature

1. Introduction

Carbon nanotubes (CNT) [1,2] have unique structure (the highly preferred orientation of their graphitic basal planes is parallel to the axis [3]) and exhibit solid lubricity. Therefore, the tribological properties of CNT composites such as resin/CNT [4-8], ceramic/CNT [9-11], and metal/CNT [12] have been studied extensively. Metal/CNT composite coatings [13-17] are particularly promising as a friction abrasion resistance technology for a wide range of applications. We have also reported the fabrication of metal/CNT composite films [18-21] and their superior frictional properties [22-24]. Previous research concerning the tribological properties of metal/CNT composite films has focused on the room temperature frictional properties. Kedward et al. reported that cobalt composite films, with WC, SiC, Cr_3C_2, and ZrB_2 as composite particles, exhibited superior wear resistance over nickel composite films, especially at high temperatures [25]. Therefore, cobalt (Co)/CNT composite films are also expected to be attractive materials with improved frictional properties not only at room temperature, but also at high temperature. However, there have been no reports on the tribological properties of Co/CNT composite plating films.

In this study, Co/CNT composite films were fabricated using an electrodeposition technique and the frictional and wear properties were evaluated at both room temperature and elevated temperatures.

2. Experimental

2.1. Chemicals

Three different sized multiwalled CNTs (MWCNTs) were used in the present study. These commercially available MWCNTs included VGCF (Showa Denko Co. Ltd.), VGCF-S (Showa Denko Co. Ltd.), and MWNT-7 (Mitsui & Co., Ltd.), the specifications of which are given in Table 1. Special grade $CoSO_4 \cdot 7H_2O$, NaCl, NaOH, and H_3BO_3 (Wako Pure Chemical Industries, Ltd) and first grade polyacrylic acid (PA5000; Wako Pure Chemical Industries, Ltd.; mean molecular weight of 5000) were used in this study. Pure water from a water purifier (RFP343RA, Advantec MFS, Inc.) was used in all experiments.

2.2. Fabrication of Co/MWCNT composite films

A solution of 1.78 M $CoSO_4 \cdot 7H_2O$ + 0.26 M NaCl + 0.57 M H_3BO_3 [25] was used as the base plating bath. The MWCNTs are hydrophobic and therefore were not uniformly dispersed in the base plating bath. A homogeneous dispersion of the

MWCNTs was achieved by the addition of PA5000 to the base plating bath with stirring. The compositions of the composite plating baths are given in Table 2. Electrodeposition of the Co/MWCNT composite films and a cobalt film was performed at 50 °C with agitation by bubbling air under galvanostatic conditions (2.5 A dm^{-2} for the Co/MWCNT composite films, 5 A dm^{-2} for the cobalt film) using a commercially available electrolytic cell (Model I, Yamamoto-Ms Co., Ltd.) with internal dimensions of 65×65×95 mm^3. The volume of the plating bath was 300 cm^3. Copper (B-60-P05, Yamamoto-Ms Co., Ltd.) and iron plates (B-60-P01, Yamamoto-Ms Co., Ltd.) with exposed surface areas of 10 cm^2 (3×3.33 cm) were used as the cathodes for characterization of the microstructures and evaluation of the tribological properties, respectively. A cobalt plate (A-53-M1-P08-19, Yamamoto-Ms Co., Ltd.) was used as the anode. Electrodeposition performed with 900 C of electricity (90 C cm^{-2}) resulted in approximately 20 μm thick films.

2.3. CNT content of Co/MWCNT composite films

The content of MWCNTs in the composite films was weighed directly. For the weight measurement, approximately >2 g of Co/MWCNT composite film was electrodeposited

(300 C cm^{-2}) on stainless substrates. After electrodeposition, the composite films were exfoliated from the stainless substrates and the cobalt matrix of the composite films was dissolved in nitric acid. The MWCNTs were filtrated from the nitric acid solution, dried and weighed. The MWCNT content was calculated as mass%, volume%, and as MWCNT number density. To calculate the volume%, the actual nanostructures of the MWCNTs were first analyzed using scanning transmission electron microscopy (STEM; HD-2300A, Hitachi). Each MWCNT had a cylindrical appearance and a hollow core with a diameter of 3-4 nm. Compared to the volume of an entire single MWCNT, that of the hollow core is negligible. Therefore, the volume% of MWCNTs in the composite film was calculated using the density of graphite (2.26 g cm^{-3}). To calculate the MWCNT number density (the number of MWCNTs per 1 g of composite film), each single MWCNT volume was calculated assuming a columnar shape of a single MWCNT using the dimensions given in Table 1. The mass of each single MWCNT was calculated using the density of graphite (2.26 g cm^{-3}) and the number of MWCNTs per 1 g of composite film was then calculated using the MWCNT mass% for the composite films.

2.4. Microstructure of Co/MWCNT composite films

The surface morphologies of the composite films were examined before and after the frictional tests using field emission-scanning electron microscopy (FE-SEM; JSM-7000F, Jeol Ltd.) with an accelerating voltage of 5 kV. A cross-section polisher (SM-09010 Jeol Ltd.) was used to prepare cross-sectional samples for FE-SEM observations. The phase structures of the composite films were evaluated before and after frictional tests using X-ray diffraction analysis (XRD; XRD-6000, Shimadzu Seisakusho) with Cu K_α radiation.

2.5. Friction and wear properties of Co/MWCNT composite films

The frictional properties of the Co/MWCNT composite films were measured using a ball-on-disk type friction test machine (High Temperature Tribometer THT1000, CSM Instruments Co.). An alumina ball (6 mm diameter, Hv=1500) was used as the counter-surface. A test load of 2 N was used with a rotation speed of 1.0 cm s^{-1} a 2 mm radius of rotation was 2 mm, and 1000 rotations (the sliding distance was 12.56 m). Tests were conducted without the use of lubricants and under ambient conditions from room temperature to 500 °C. The coefficient of friction was measured continuously

using a load cell during the tests. The wear volume was calculated from the cross-sectional areas of wear scars, which were measured using a roughness meter (Surtronic 25, Taylor Hobson Co.). The wear rate was calculated using the wear volume, the test load (2 N), and the sliding distance (12.56 m).

3. Results and discussion

3.1. Surface and cross-sectional morphology of Co/MWCNT composite films

Fig. 1 shows surface and cross-sectional SEM images of the electrodeposited Co/MWCNT composite films. SEM images of a cobalt film are also shown (Figs. 1a, 1e) for comparison. Bare individual MWCNTs are distributed homogeneously at the surface of every Co/MWCNT composite film (Figs. 1 b-d). The black areas in the cross-sectional SEM images are MWCNTs (Figs. 1f-1h). There are no gaps and voids in the cross-sections of the films, which indicates that the composite films have compact structures. The MWCNTs are distributed individually and homogeneously throughout the composite films, so that the microstructure of the composite films in the depth direction is the same as that of the surface.

3.2. MWCNT content in composite films

The MWCNT contents in the composite films are presented in Table 3. The order of MWCNT mass% and volume% for the Co/MWCNT composite films is Co/VGCF > Co/VGCF-S > Co/MWNT-7; the volume% (mass%) of the Co/VGCF composite film is approximately 3 times higher than the other composite films. However, the MWCNT number densities of the composite films are almost the same ($1.0\text{-}1.7\times10^{10}$).

3.3. Friction and wear properties of Co/MWCNT composite films

3.3.1 Friction and wear properties at room temperature

Fig. 2 shows the frictional behavior of the Co/MWCNT composite films at room temperature, in addition to that of a cobalt film for comparison. The cobalt film has a coefficient of friction of ca. 0.3 from the beginning to the end of the wear test. The coefficients of friction of the Co/MWCNT composite films are lower than that of the cobalt film. The coefficients of friction of the Co/MWNT-7 and Co/VGCF-S composite films increased gradually from initial values of 0.15 and 0.16 to final values of 2.8 and

1.9, respectively. In contrast, the coefficient of friction of the Co/VGCF composite film remained constant at ca. 0.11 during the wear test. Thus, the order of lower coefficient of friction for the composite films with respect to the cobalt film is Co/VGCF > Co/VGCF-S > Co/MWNT-7, and the Co/VGCF composite film showed the lowest coefficient of friction. The MWCNT number densities of the composite films were almost the same, whereas the order for the MWCNT volume% in the composite films was Co/VGCF > Co/VGCF-S > Co/MWNT-7. Therefore, the coefficients of friction may be related not with the number density, but with the volume% of MWCNTs in the composite films. Although the type of MWCNTs may affect the frictional properties, the MWCNTs used in the present study are all graphitized, so that the effect on the coefficient of friction is considered to be negligible [23]. The contact area between the MWCNTs and the alumina counter surface increases with the volume% of MWCNTs, so that the contact area between the cobalt matrix and alumina counter surface decreases with increase in the volume% of MWCNTs, which results in a lower coefficient of friction than the cobalt film. There have been many reports on coefficient of friction measurements for only MWCNTs [26-32]. Dickrell et al. reported the coefficients of friction of vertically and transversely aligned MWCNTs as 0.795 and 0.090, respectively, using a borosilicate glass pin as a counter surface under ambient conditions

[27]. The coefficients of friction of all the composite films at initial stage were 0.1-0.15 in the present work, which is similar to the coefficient of friction of 0.090 for only MWCNTs, which suggests that the side walls of the MWCNTs act as effective solid lubricants. When the wear test starts, the alumina ball scratches the Co/MWCNT composite film, and the surface, especially the cobalt matrix, is plastically deformed, which results in the transverse arrangement of the MWCNTs [22]. This is another reason that the Co/MWCNT composite films have lower coefficients of friction than the cobalt film. The volume% of MWCNTs in the Co/VGCF-S and Co/MWCNT-7 composite films may not be sufficient to lower the coefficient of friction; therefore, their coefficients of friction increased gradually toward the coefficient of friction of the cobalt film (0.3) with increase in the sliding distance. In contrast, the volume% of MWCNTs in the Co/VGCF composite film is sufficient, which resulted in a constant low coefficient of friction of around 0.11, which is similar to that of transversely aligned MWCNTs (0.09).

SEM images of the wear scars on the films after the wear test (12.56 m sliding distance) are shown in Fig. 3. A clear, continuous, and wide-width scar is evident on the surface of the cobalt film (Fig. 3a). In contrast, the wear scars of the composite films are discontinuous and their widths are less than that of the cobalt film. This indicates that

the contact areas between the composite films and the alumina counter surface are smaller than that between the cobalt film and the counter surface. The wear area appears to be the smallest for the Co/VGCF composite film, which correlates well with the frictional properties measured at room temperature. The wear scars obtained at room temperature were very shallow, which made an exact comparison difficult; therefore, the data for the wear rates at room temperature are not given here. The Co/VGCF composite film, which had the lowest coefficient of friction at room temperature, was used as a sample for friction and wear tests at elevated temperatures.

3.3.2 Friction and wear properties at elevated temperatures

Fig. 4b shows the frictional behavior of the Co/VGCF composite film at various temperatures, in addition to that of the cobalt film for comparison (Fig. 4a). The coefficient of friction of the cobalt film increased with the temperature. The increase in the coefficient of friction was not proportional to the temperature in the range of 100-400 °C, but rapidly increased at 500 °C. The fluctuation of the coefficient of friction in the range of 100-400 °C is very large. The coefficient of friction of the Co/VGCF composite film also increased with the temperature, rapidly at 100 °C, gradually between 100 and 400 °C, and then rapidly at 500 °C. The fluctuation of the

coefficient of friction in the range of 200-400 °C was large and similar to that for the cobalt film. The Co/VGCF composite film had a slightly lower coefficient of friction than the cobalt film at elevated temperatures (100-500 °C).

SEM images of the wear scars on the cobalt film after wear testing at elevated temperatures are shown in Fig. 5. Compared to the wear scar width obtained at room temperature (Fig. 5a), those obtained at up to 300 °C (Figs. 5b and 5c) were wider, and the width of the wear scar at 400 °C was similar to that obtained at 300 °C. In contrast, the width of the wear scar obtained at 500 °C was smaller than those obtained at 200 °C and 300 °C, and was almost the same width as that obtained at room temperature (Fig. 5d). Fig. 6 shows SEM images of the wear scars obtained for the Co/VGCF composite film at various temperatures. The wear scar width increased compared to that obtained at room temperature (Fig. 6a), up to 300 °C (Fig. 6b, 6c). The width of the wear scar at 400 °C was similar to that obtained at 300 °C. However, the width of the wear scar at 500 °C was smaller than that obtained at 200 and 300 °C, and was almost the same as that obtained at room temperature (Fig. 6d). Thus, the variations of the wear scar width for both the cobalt and Co/VGCF composite films were similar at elevated temperatures.

Fig. 7 shows the wear rate as a function of the temperature for the cobalt film and

the Co/VGCF composite film. The wear rates of both films increased with the temperature up to 300 °C and then decreased with further increase in the test temperature. The variations of the wear rates for the cobalt film and the Co/VGCF composite film were consistent with the wear scar widths shown in Figs. 5 and 6. However, comparing the results in Fig. 4 with those in Figs. 5-7 does not reveal a good correlation between the frictional properties and the wear properties at elevated temperatures.

To determine the variation between the frictional properties and the wear rate of the Co/VGCF composite film at elevated temperatures, the microstructures of the films were evaluated after wear tests at various temperatures. Fig. 8 shows surface SEM images of the cobalt film near the wear scars after wear tests at various temperatures. Electrodeposited grains of several micrometers in diameter were observed on the surface of the cobalt film at room temperature (Fig. 8a). The surface morphology of the films near the wear scars after the wear tests at 100 and 200 °C was almost the same as that at room temperature; however, a change in the surface morphology was evident above 300 °C. At 300 °C, the surface morphology appeared to be slightly uneven, compared with that obtained below 200 °C (Fig. 8b). A plate-like morphology appeared on the surface of the cobalt film at 400 °C (Fig. 8c), and the surface became smoother

with a lesser amount of the plate-like morphology at 500 °C (Fig. 8d).

Fig. 9 shows surface SEM images of the Co/VGCF composite film near the wear scars after wear tests at various temperatures. Much of the VGCF incorporated partially in the cobalt matrix was observed on the surface of the film at room temperature (Fig. 9a). The cobalt grain sizes were approximately 1 μm in diameter. At elevated temperatures, the surface morphology of the cobalt matrix changed in a similar way to that for the cobalt film; a slightly uneven morphology appeared at 300 °C (Fig. 9b) and a plate-like morphology was observed at 400 °C (Fig. 9c), while the surface became smoother at 500 °C (Fig. 9d). The number of VGCFs on the surface was significantly decreased and there were almost no VGCFs on the surface at 500 °C (Fig. 9d).

Fig. 10 shows XRD patterns for the cobalt film after the wear tests at various temperatures. Diffraction peaks assigned to close-packed hexagonal cobalt were observed at room temperature and 300 °C (Figs. 10a and 10b). In addition to the close-packed hexagonal cobalt peaks, a diffraction peak assigned to Co_3O_4 was observed at 400 °C (Fig. 10c) and the intensity of the Co_3O_4 peak increased at 500 °C (Fig. 10d). Fig. 11 shows XRD patterns of the Co/VGCF composite film after the wear tests at various temperatures. The phase structures of the Co/VGCF composite films were almost the same as those of the cobalt film, with diffraction peaks assigned to

close-packed hexagonal cobalt observed at room temperature and up to 300 °C (Figs. 11a and 11b). A diffraction peak assigned to Co_3O_4 was also observed in addition to the close-packed hexagonal cobalt peaks at 400 °C (Fig. 11c), and the intensity of the Co_3O_4 peaks increased at 500 °C (Fig. 11d). Therefore, the morphological changes on the surface of the cobalt matrix of the Co/VGCF composite film are due to the formation of cobalt oxides such as the Co_3O_4. Diffraction peaks assigned to MWCNTs were not observed in every diffraction pattern in Fig. 11, due to low quantities of MWCNTs. Although no clear peaks to indicate the presence of cobalt oxides were observed in the XRD patterns of the Co/VGCF composite film or the cobalt film at 100 and 200 °C, a larger quantity of cobalt oxides should be formed at 100 and 200 °C than that at room temperature. Fig. 12 shows a cross-sectional SEM image of the Co/VGCF composite film near the wear scar after wear testing at 500 °C. A continuous layer of around 1 μm thick is observed on the Co/VGCF composite film, which is considered to be a Co_3O_4 layer. A comparison of the results in Figs. 4 and 7 with those Figs. 8-12 suggests the variations of the coefficients of friction and wear rates for the Co/VGCF composite film at elevated temperatures are related to the formation of cobalt oxides such as Co_3O_4 and the dissipation of MWCNTs. The amount of cobalt oxides formed on the surface of the Co/VGCF composite film should increase with increasing temperature.

At the sliding surface, the removal of surface oxides and the formation of oxides on the bare cobalt surface, on which oxidation rate must be very high, occur repeatedly during the wear test. This results in the formation of a significant amount of abrasive cobalt oxide powders on the sliding surface; therefore, the coefficient of friction increases at elevated temperatures. However, the removal of abrasive powders from the sliding surface may occur, depending on the temperature, which results in relatively large fluctuations of the coefficient of friction.

Compared to the cobalt film, the Co/VGCF composite film had a slightly lower coefficient of friction due to the solid lubricity of the MWCNTs. The coefficient of friction increased abruptly at 500 °C, compared to that of 400 °C, because the MWCNTs almost disappeared from the surface of the Co/VGCF composite film and cobalt oxides were formed. The wear rates of the Co/VGCF composite film increased with increasing temperature up to 300 °C, due to increasing cobalt oxide formation, most of which are easily removed from the sliding surface by the alumina counter surface. At 400 °C, a significant amount of abrasive cobalt oxide powders may remain and act as a protective layer on the sliding surfaces, which results in a reduction of the wear rate. At 500 °C, the cobalt oxide layer becomes more protective, and combined with the dissipation of MWCNTs, results in a wear rate that is similar to that for the

cobalt film at 500 °C. The change in the hardness of the composite films at elevated temperatures may affect the frictional and wear properties of the composite films, and such effects will be investigated in future work.

Finally, we discuss the reason for the disappearance of the MWCNTs from the surface of the Co/VGCF composite film. Fig. 13 shows the Co-C binary alloy phase diagram. According to the phase diagram, the stable phase of cobalt up to 422 °C is close-packed hexagonal, above which the stable phase changes to face-centered cubic. In the XRD patterns of the films at 500 °C (Figs. 10d and Fig. 11d), no diffraction peaks assigned to face-centered-cubic cobalt are observed, the reason for which will also be studied in future work. Note that carbon does not dissolve in close-packed hexagonal cobalt to form a solid solution. However, carbon does dissolve slightly in face-centered cubic cobalt, although the solubility limit of carbon in cobalt is very low at 500 °C. Therefore, MWCNTs are considered to not react with the cobalt matrix during the wear test at any of the temperatures measured in this work (from room temperature to 500 °C). MWCNTs were present in the composite films after the wear test at 500 °C (Fig. 12); therefore, the dissolution of MWCNTs into the cobalt matrix is not related with the dissipation of MWCNTs from the surface of the Co/VGCF composite film. MWCNTs are known to be oxidized in the air at elevated temperatures [33,34]. Bom et

al. reported that raw MWCNTs were oxidized above 400-450 °C, and MWCNTs graphitized at 2800 °C were more thermally stable than the raw MWCNTs and were oxidized above 600 °C [35]. The VGCFs used in the present study were MWCNTs that were graphitized at 2800 °C. Therefore, these VGCFs should not be oxidized below 500 °C, i.e., the VGCFs should not disappear below 500 °C. It is considered that cobalt or cobalt oxide on the surface of the composite film may have a catalytic effect on the oxidation of the VGCFs. However, the exact reason for the disappearance of the VGCFs at 500 °C has yet to be clarified, and this will be examined in future work.

4. Conclusions

Co/MWCNT composite films were fabricated using an electrodeposition technique and their frictional and wear properties were examined. The Co/MWCNT composite films had lower coefficients of friction than cobalt film at room temperature. At elevated temperatures, the coefficients of frictional of the composite films increased due to the formation of a significant amount of cobalt oxides on the surface and the dissipation of MWCNTs at 500 °C.

References

[1] A. Oberlin, M. Endo, T. Koyama, J. Cryst. Growth 32 (1976) 335.

[2] S. Iijima, T. Ichihashi, Nature 363 (1993) 603.

[3] M. Endo, Y.A. Kim, T. Hayashi, K. Nishimura, T. Matsushita, K. Miyashita, M.S. Dresselhaus, Carbon 39 (2001) 1287.

[4] W.X. Chen, F. Li, G. Han, J.B. Xia, L.Y. Wang, J.P. Tu, Z.D. Xu, Tribol. Lett. 15 (2003) 275.

[5] Y.S. Zoo, J.W. An, D.P. Lim, D.S. Lim, Tribol. Lett. 16 (2004) 305.

[6] H. Cai, F. Yan, Q. Xue, Mater. Sci. Eng., A 364 (2004) 94.

[7] A. Tanaka, K. Umeda, M. Yudasaka, M. Suzuki, T. Ohana, M. Yumura, S. Iijima, Tribol. Lett. 19 (2005) 135.

[8] O. Jacobs, W. Xu, B. Schadel, W. Wu, Tribol. Lett. 23 (2006) 65.

[9] E. Flahaut, A. Peigney, C. Laurent, C. Marliere, F. Chastel, A. Rousset, Acta Mater. 48 (2000) 3803.

[10] R.W. Siegel, S.K. Chang, B.J. Ash, J. Stone, P.M. Ajayan, R.W. Doremus, L.S. Schadler, Scr. Mater. 44 (2001) 2061.

[11] G.D. Zhan, J.D. Kuntz, J.L. Wan, A.K. Mukherjee, Nat. Mater. 2 (2003) 38.

[12] J.P. Tu, Y.Z. Yang, L.Y. Wang, X.C. Ma, X.B. Zhang, Tribol. Lett. 10 (2001) 225.

[13] W.X. Chen, J.P. Tu, L.Y. Wang, H.Y. Gan, Z.D. Xu, X.B. Zhang, Carbon 41 (2003) 215.

[14] W.X. Chen, J.P. Tu, Z.D. Xu, W.L. Chen, X.B. Zhang, D.H. Cheng, Mater. Lett. 57 (2003) 1256.

[15] X.H. Chen, C.S. Chen, H.N. Xiao, H.B. Liu, L.P. Zhou, S.L. Li, G. Zhang, Tribol. Int. 39 (2006) 22.

[16] Z.H. Li, X.Q. Wang, M. Wang, F.F. Wang, H.L. Ge, Tribol. Int. 39 (2006) 953.

[17] J. Tan, T. Yu, B. Xu, Q. Yao, Tribol. Lett. 21 (2006) 107.

[18] S. Arai, M. Endo, Electrochem. Commun. 7 (2005) 19.

[19] S. Arai, T. Saito, M. Endo, J. Electrochem. Soc. 154 (2007) D530.

[20] S. Arai, T. Saito, M. Endo, J. Electrochem. Soc. 157 (2010) D127.

[21] S. Arai, T. Saito, M. Endo, J. Electrochem. Soc. 157 (2010) D147.

[22] S. Arai, A. Fujimori, M. Murai, M. Endo, Mater. Lett. 62 (2008) 3545.

[23] S. Arai, T. Sato, M. Endo, J. Electrochem. Soc. 157 (2010) D570.

[24] S. Arai, T. Sato, M. Endo, Surf. Coat. Technol. 205 (2011) 3135.

[25] E.C. Kedward, C.A. Addison, A.A.B. Tennett, Met. Finish. 54 (1976) 8.

[26] A. Hirata, N. Yoshioka, Tribol. Int. 37 (2004) 893.

[27] P.L. Dickrell, S.B. Sinnott, D.W. Hahn, N.R. Raravikar, L.S. Schadler, P.M. Ajayan, W.G. Sawyer, Tribol. Lett. 18 (2005) 59.

[28] V. Turq, N. Ohmae, J.M. Martin, J. Fontaine, H. Kinoshita, J.L. Loubet, Tribol. Lett. 19 (2005) 23.

[29] J.J. Hu, S.H. Jo, Z.F. Ren, A.A. Voevodin, J.S. Zabinski, Tribol. Lett. 19 (2005) 119.

[30] K. Miyoshi, K.W. Street Jr., R.L. van der Wal, R. Andrews, A. Sayir, Tribol. Lett. 19 (2005) 191.

[31] P.L. Dickrell, S.K. Pal, G.R. Baurne, C. Muratore, A.A. Voevodin, P.M. Ajayan, L.S. Schadler, W.G. Sawyer, Tribol. Lett. 24 (2006) 85.

[32] N. Ohmae, Tribol. Int. 39 (2006) 1497.

[33] C. Li, D. Wang, T. Liang, X. Wang, J. Wu, X. Hu, J. Liang, Powder Technol. 142 (2004) 175.

[34] S. Osswald, M. Havel, Y. Gogotsi, J. Raman Spectrosc. 38 (2007) 728.

[35] D. Bom, R. Andrews, D. Jacques, J. Anthony, B. Chen, M.S. Meier, J.P. Selegue, Nano Lett. 2 (2002) 615.

Figure captions

Fig. 1. Surface and cross-sectional SEM images of (a,e) cobalt film, and the (b,f) Co/VGCF, (c,g) Co/VGCF-S, and (d,h) Co/MWNT-7 composite films.

Fig. 2. Variation in coefficient of friction as a function of the sliding distance for the cobalt and Co/MWCNT composite films at room temperature: ●: cobalt film, ○: Co/VGCF composite film, □: Co/VGCF-S composite film, △: Co/MWNT-7 composite film.

Fig. 3. Surface SEM images of wear scars on the films after room temperature wear tests. (a) Cobalt film, and the (b) Co/VGCF, (c) Co/VGCF-S, and (d) Co/MWNT-7 composite films.

Fig. 4. Variation in coefficient of friction as a function of sliding distance for the (a) cobalt film and (b) Co/VGCF composite film at various temperatures: ●: room temperature, ○: 100 °C, ◎: 200 °C, □: 300 °C, ◇: 400 °C, and: △ 500 °C

Fig. 5. Surface SEM images of wear scars on the cobalt film after wear tests at (a) room temperature, (b) 200, (c) 300, and (d) 500 °C. The sliding distance was 12.56 m.

Fig. 6. Surface SEM images of wear scars on the Co/VGCF composite film after wear tests at (a) room temperature, (b) 200, (c) 300, and (d) 500 °C. The sliding distance was 12.56 m.

Fig. 7. Wear rate of the cobalt film and the Co/VGCF composite film as a function of temperature. The sliding distance was 12.56 m.

Fig. 8. Surface SEM images of the cobalt film near the wear scars after wear tests at (a) room temperature, (b) 300, (c) 400, and (d) 500 °C.

Fig. 9. Surface SEM images of the Co/VGCF composite film near the wear scars after wear tests at (a) room temperature, (b) 300, (c) 400, and (d) 500 °C.

Fig. 10. XRD patterns of the cobalt film after wear tests at (a) room temperature, (b) 300, (c) 400, and (d) 500 °C.

Fig. 11. XRD patterns of the Co/VGCF composite film after wear tests at (a) room temperature, (b) 300, (c) 400, and (d) 500 °C.

Fig. 12. Cross-sectional SEM image of the Co/VGCF composite film after the wear test at 500 °C.

Fig. 13. Co-C binary alloy phase diagram from Ref. [29].

Table(1)

Table 1　Specifications of MWCNTs.

MWCNT	Diameter (nm)	Length (μm)
VGCF	100 – 150	10 – 15
VGCF-S	80	10 – 15
MWNT-7	60	10 – 15

Table(2)

Table 2　Compositions of the plating baths.

Reagents	Cobalt	Co/VGCF	Co/VGCF-S	Co/MWNT-7
$CoSO_4 \cdot 7H_2O$	1.78 M	1.78 M	1.78 M	1.78 M
NaCl	0.26 M	0.26 M	0.26 M	0.26 M
H_3BO_3	0.57 M	0.57 M	0.57 M	0.57 M
PA5000		2×10^{-5} M	2×10^{-5} M	2×10^{-5} M
MWCNT		1.5 g dm^{-3}	0.8 g dm^{-3}	0.55 g dm^{-3}

Table(3)

Table 3 MWCNT contents in the composite films.

Co/MWCNT composite film	Mass%	Vol%	MWCNT number density (number per 1 g of composite)
Co/VGCF composite film	0.51	2.17	1.2×10^{10}
Co/VGCF-S composite film	0.17	0.73	1.0×10^{10}
Co/MWNT-7 composite film	0.15	0.65	1.7×10^{10}

Figure(1)

Click here to download Figure(s): Figure1.pptx

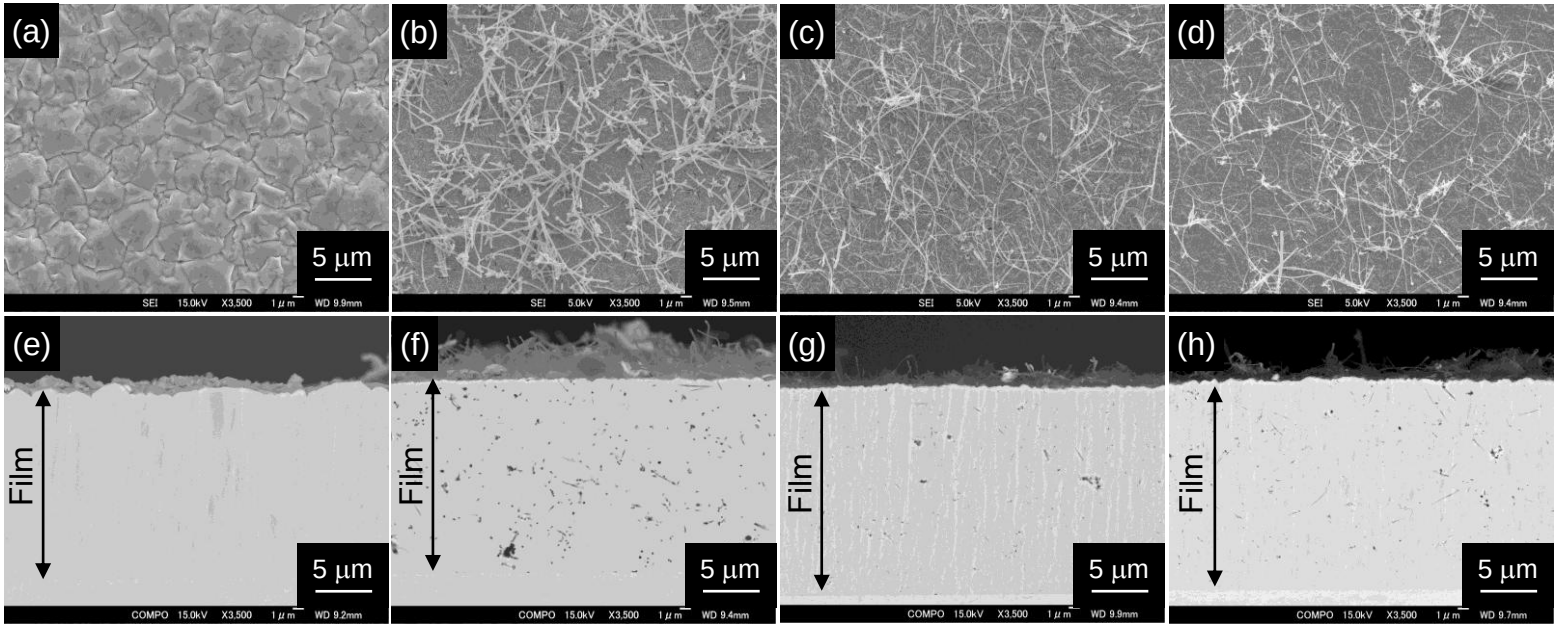

Fig. 1

Figure(2)
Click here to download Figure(s): Figure2.pptx

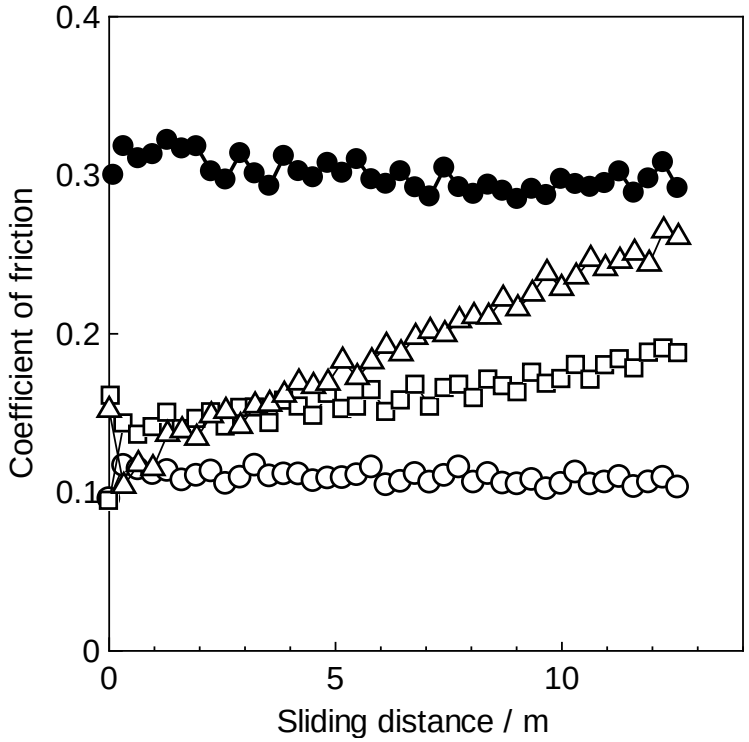

Fig. 2

Figure(3)
Click here to download Figure(s): Figure3.pptx

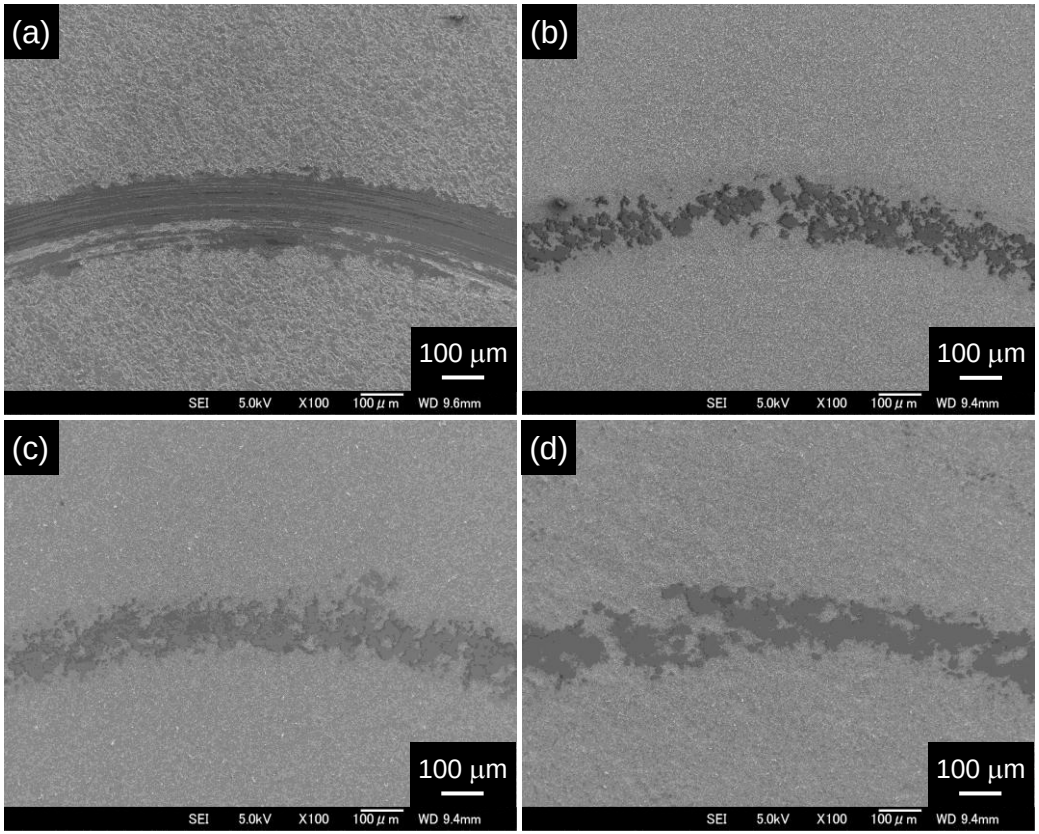

Fig. 3

Figure(4)

Click here to download Figure(s): Figure4.pptx

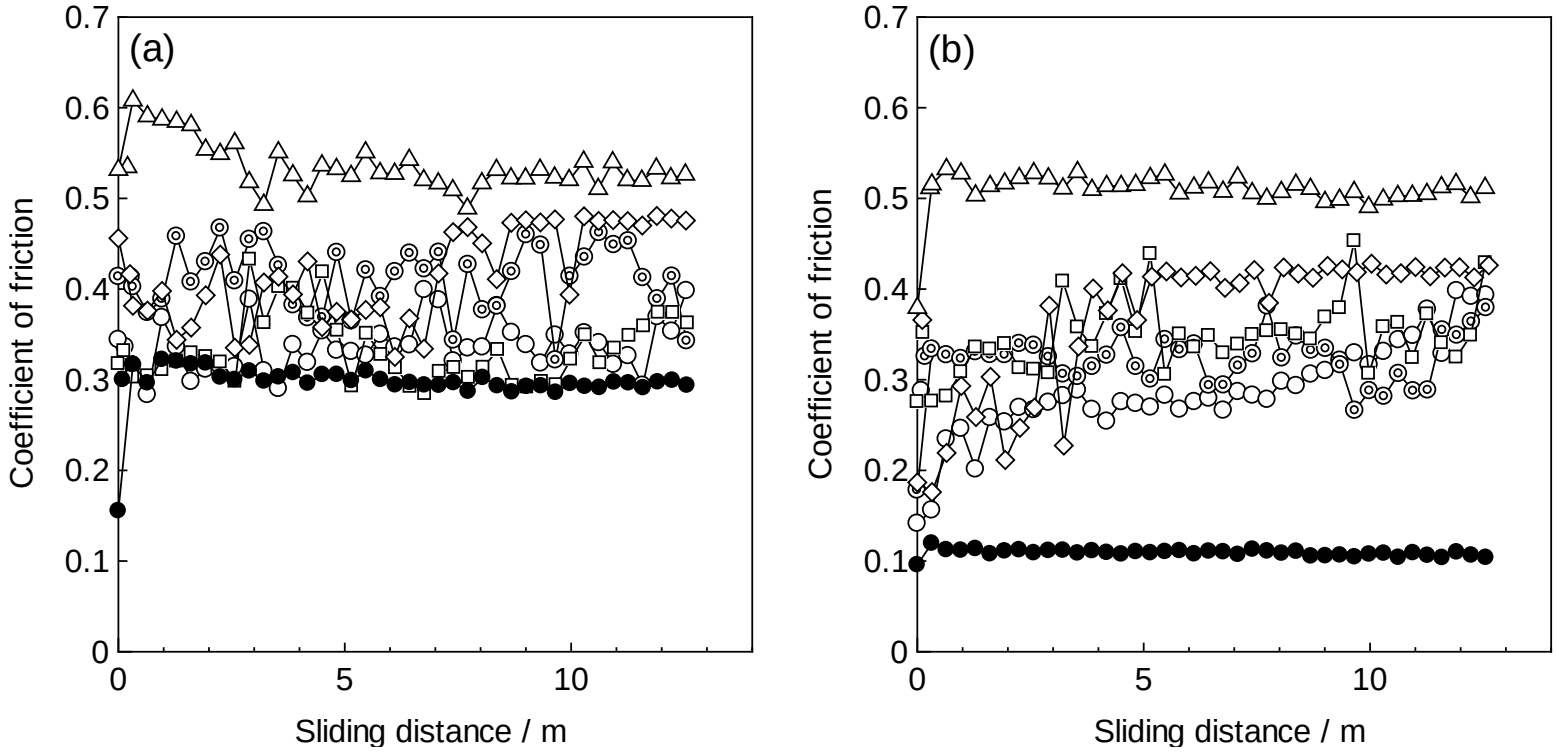

Fig. 4

Figure(5)

Click here to download Figure(s): Figure5.pptx

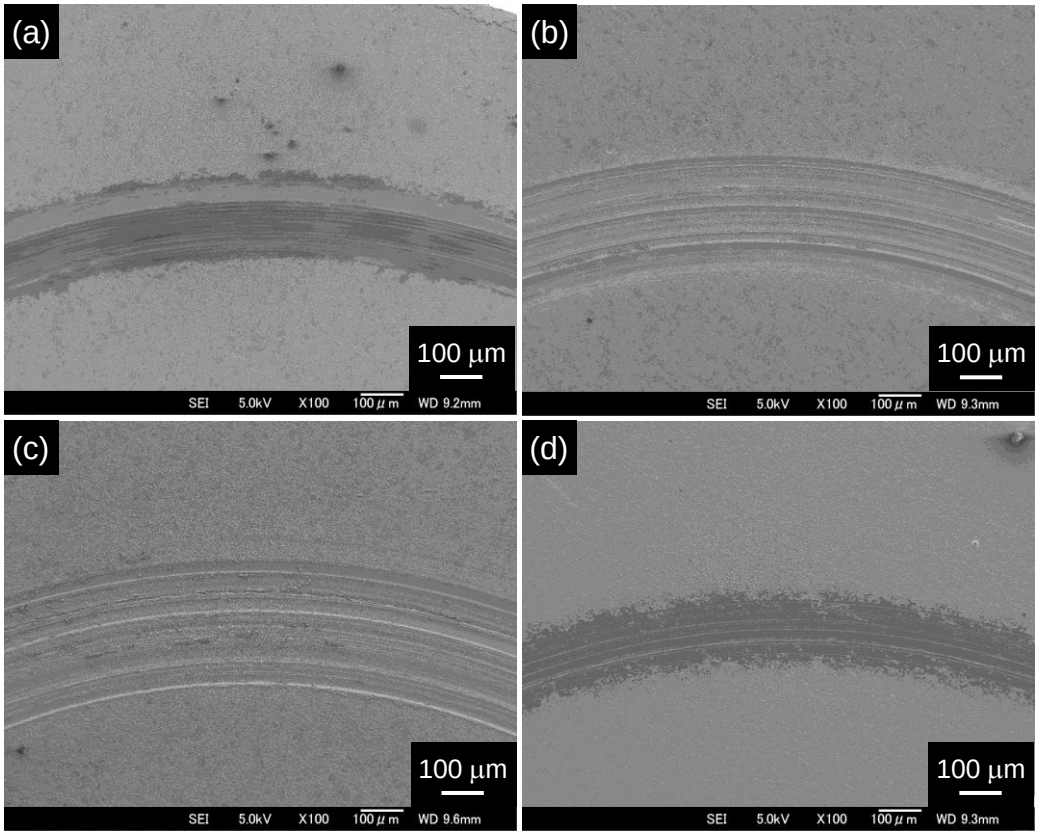

Fig. 5

Figure(6)

Click here to download Figure(s): Figure6.pptx

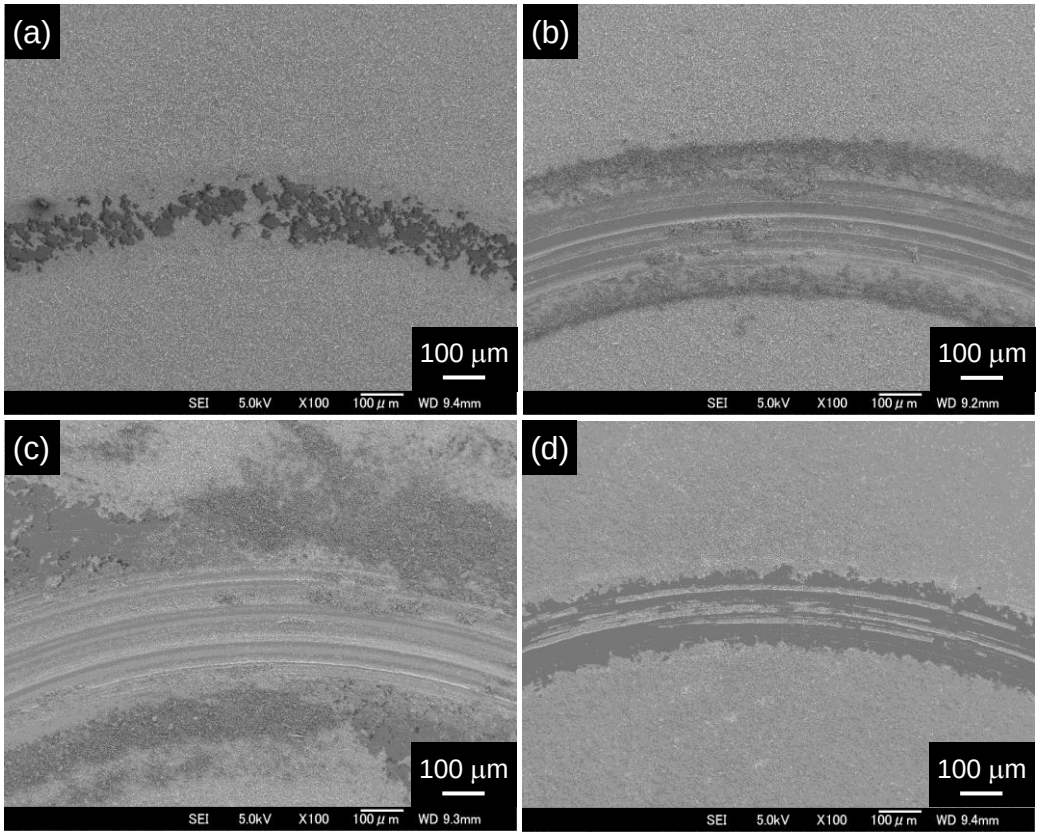

Fig. 6

Figure(7)
Click here to download Figure(s): Figure7.pptx

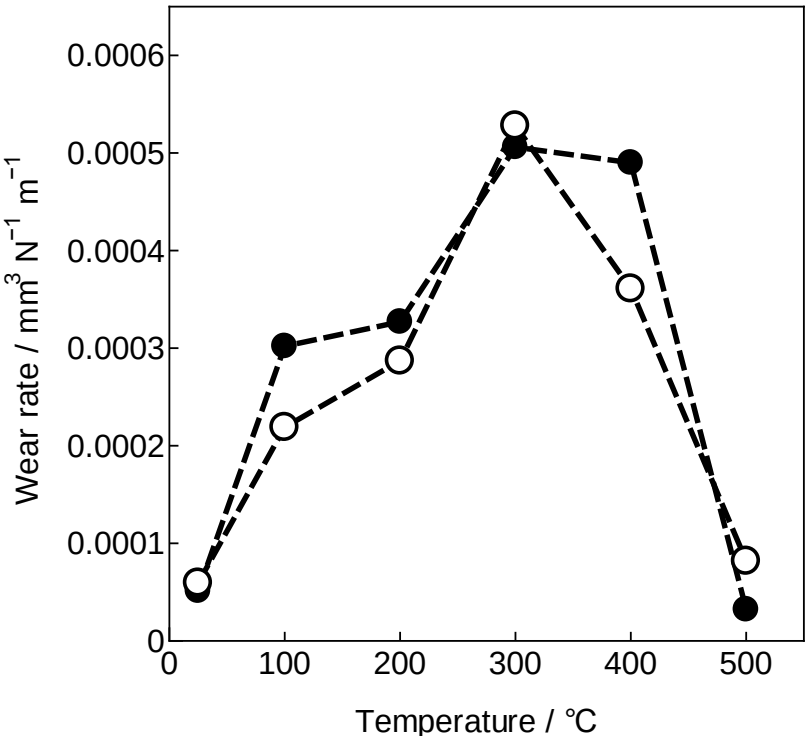

Fig. 7

Figure(8)

Click here to download Figure(s): Figure8.pptx

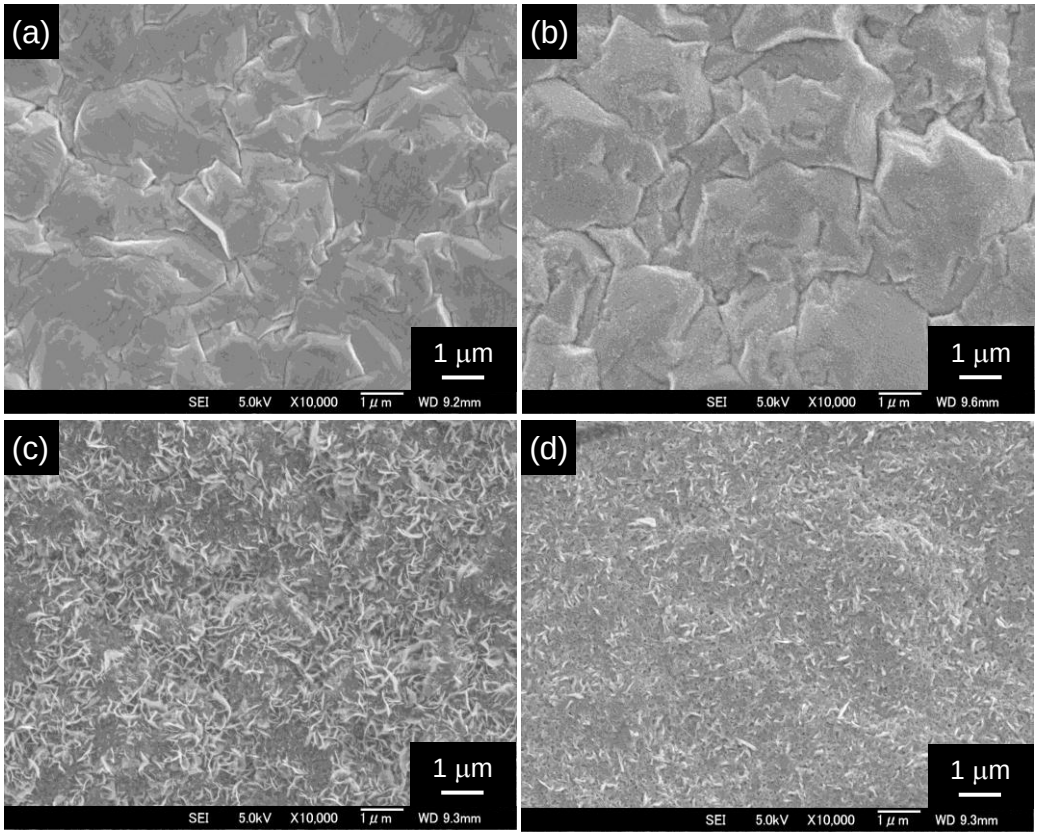

Fig. 8

Figure(9)
Click here to download Figure(s): Figure9.pptx

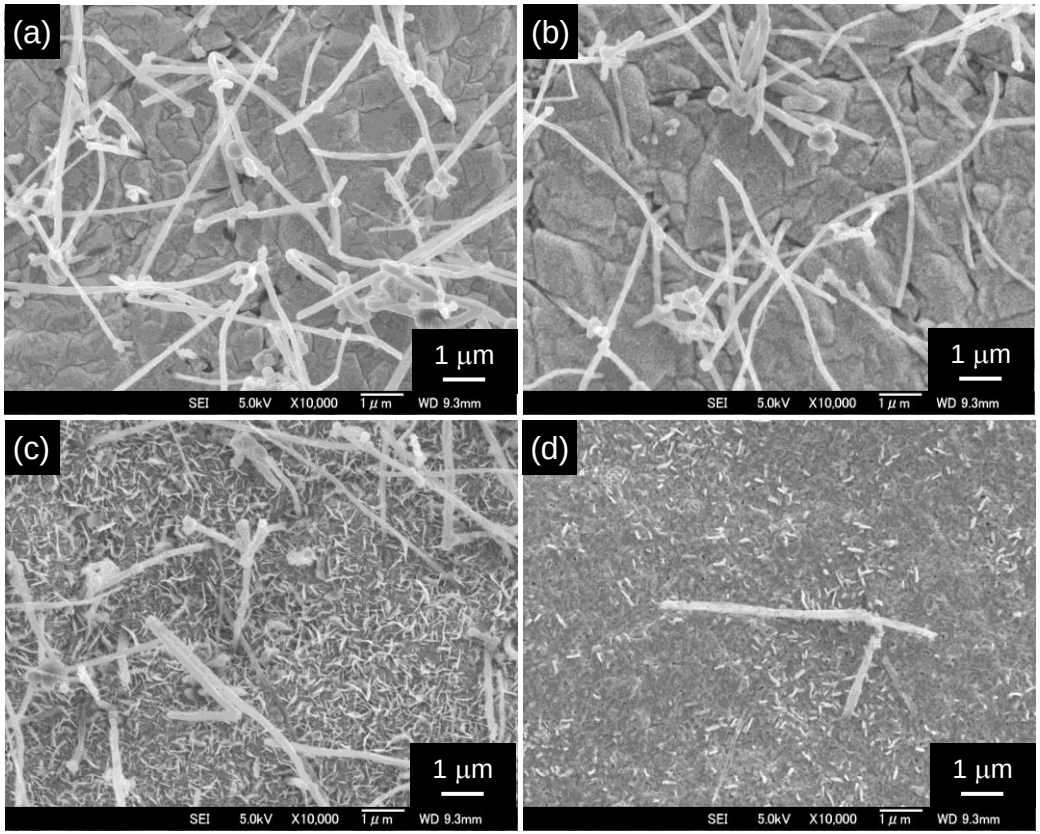

Fig. 9

Figure(10)

Click here to download Figure(s): Figure10.pptx

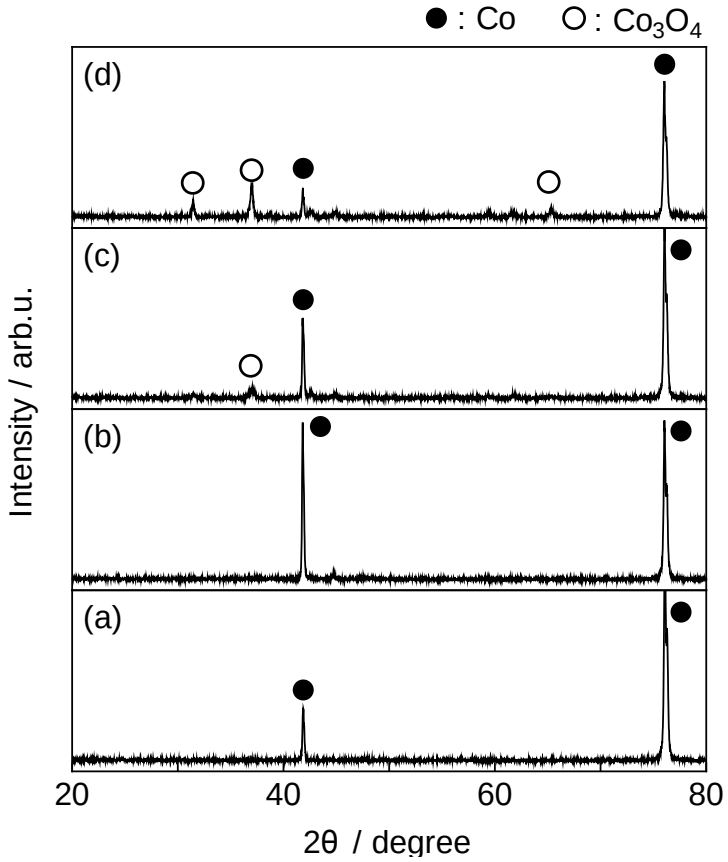

Fig. 10

Figure(11)

Click here to download Figure(s): Figure11.pptx

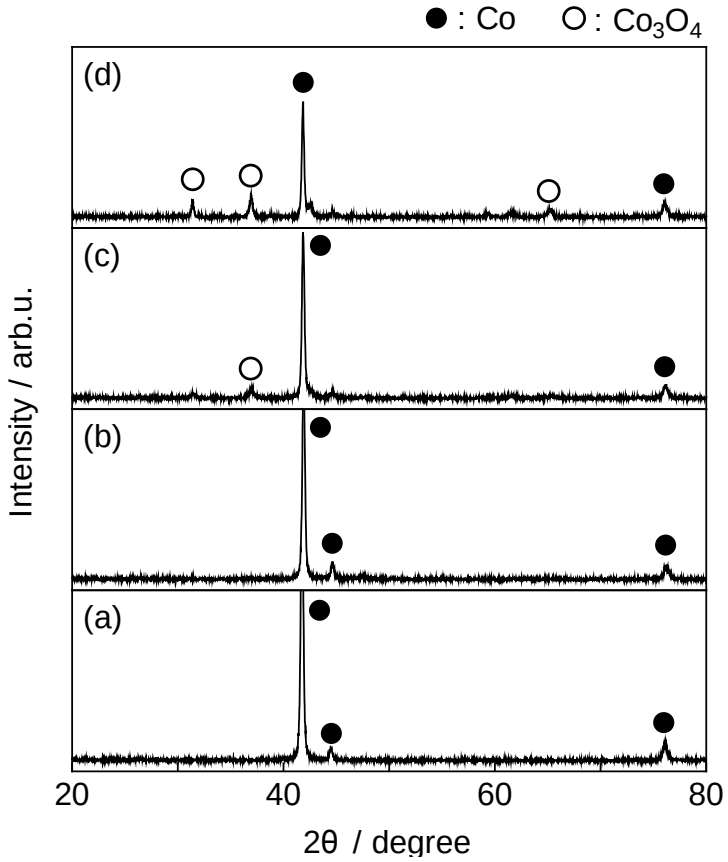

Fig. 11

Figure(12)

Click here to download Figure(s): Figure12.pptx

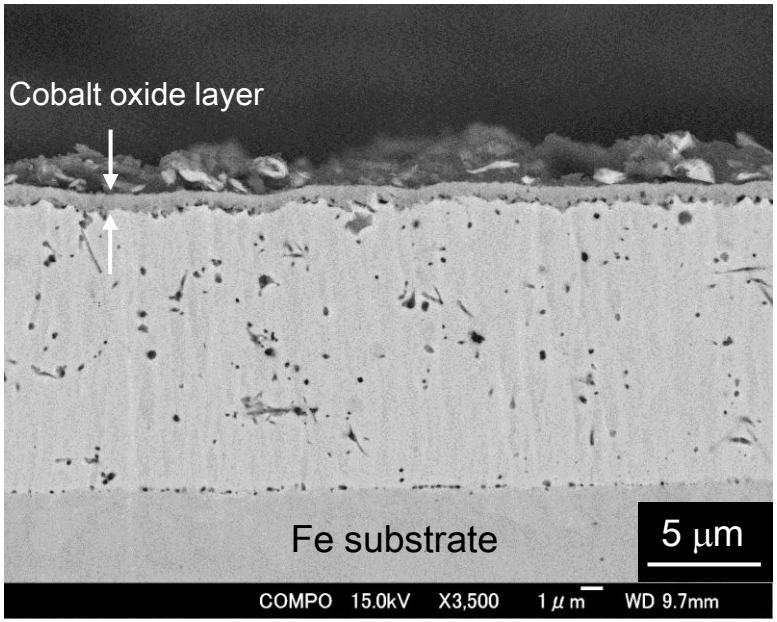

Fig. 12

Figure(13)

Click here to download Figure(s): Figure13.pptx

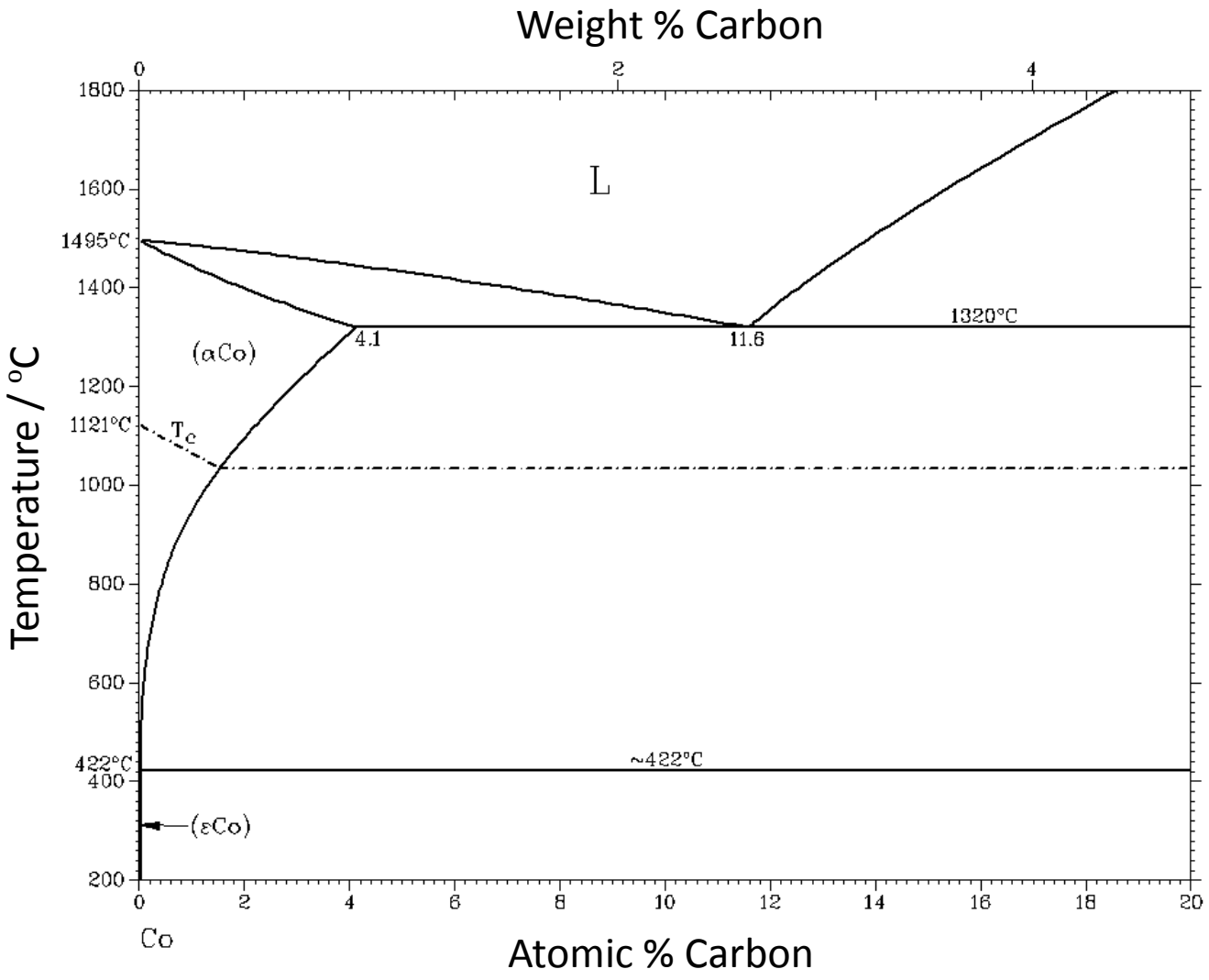

Fig. 13